Plasmonic dimer antennas for surface enhanced Raman scattering



2012 Nanotechnology 23 185303

(http://iopscience.iop.org/0957-4484/23/18/185303)

Nanotechnology **23** (2012) 185303 (7pp) doi:10.1088/0957-4484/23/18/185303

# Plasmonic dimer antennas for surface enhanced Raman scattering

**Katja Höflich[1,2], Michael Becker[1], Gerd Leuchs[3,4] and Silke Christiansen[2,3]**

[1] Max Planck Institute of Microstructure Physics, Weinberg 2, D-06120 Halle, Germany
[2] Institute of Photonic Technology, Albert-Einstein-Straße 9, D-07745 Jena, Germany
[3] Max Planck Institute for the Science of Light, Günther-Scharowsky-Straße 1, D-91058 Erlangen, Germany
[4] University Erlangen–Nuremberg, Institute of Optics, Information and Photonics, Staudtstraße 7/B2, D-91058 Erlangen, Germany

E-mail: katja.hoeflich@mpl.mpg.de

Received 20 December 2011, in final form 24 February 2012
Published 13 April 2012
Online at stacks.iop.org/Nano/23/185303

**Abstract**
Electron beam induced deposition (EBID) has recently been developed into a method to directly write optically active three-dimensional nanostructures. For this purpose a metal–organic precursor gas (here dimethyl-gold(III)-acetylacetonate) is introduced into the vacuum chamber of a scanning electron microscope where it is cracked by the focused electron beam. Upon cracking the aforementioned precursor gas, 3D deposits are realized, consisting of gold nanocrystals embedded in a carbonaceous matrix. The carbon content in the deposits hinders direct plasmonic applications. However, it is possible to activate the deposited nanostructures for plasmonics by coating the EBID structures with a continuous silver layer of a few nanometers thickness. Within this silver layer collective motions of the free electron gas can be excited. In this way, EBID structures with their intriguing precision at the nanoscale have been arranged in arrays of free-standing dimer antenna structures with nanometer sized gaps between the antennas that face each other with an angle of 90°. These dimer antenna ensembles can constitute a reproducibly manufacturable substrate for exploiting the surface enhanced Raman effect (SERS). The achieved SERS enhancement factors are of the order of $10^4$ for the incident laser light polarized along the dimer axes. To prove the signal enhancement in a Raman experiment we used the dye methyl violet as a robust test molecule. In future applications the thickness of such a silver layer on the dimer antennas can easily be varied for tuning the plasmonic resonances of the SERS substrate to match the resonance structure of the analytes to be detected.

(Some figures may appear in colour only in the online journal)

## 1. Introduction

Raman spectroscopy has been shown to be a practicable application in the field of plasmonics [1]. Standard Raman spectroscopy permits us to accurately measure characteristic frequencies of molecular vibrations. However, the Raman scattering cross section is extremely small ($\approx 10^{-31}$ – $10^{-29}$ cm$^2$ per molecule [2]) compared to other spectroscopic techniques such as infrared spectroscopy. This small Raman scattering cross section can be increased by many orders of magnitude, when the analytes reside on metallic surfaces with roughnesses at the nanoscale. In this case, which is often called surface enhanced Raman spectroscopy (SERS), two enhancement mechanisms are responsible. The most important mechanism is the electromagnetic field enhancement in the vicinity of nanosized metal particles and clusters due to the excitation of plasmonic surface modes by the incident visible light. In particular, the surface plasmon modes of closely spaced metal nanoparticles interact strongly and lead to so-called hotspots. This interaction,

 

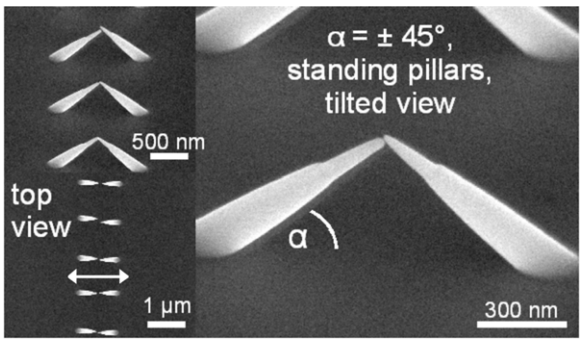


**Figure 1.** Scanning electron micrographs of EBID pillars arranged in the form of dimer antennas optimized for SERS applications. The two pillars forming the dimer antennas form an angle of 45° with respect to the Si substrate surface; the dimer axis is indicated by the double-headed arrow in the top view. The gap spacings in between the pillar tips can be reduced to approximately 5 nm in width and constitute the hotspot region for maximum electric field enhancement.

which explains the observed giant Raman enhancements on the order of $10^{12}$ [3, 4], is most efficient for gaps as small as a few nanometers due to the evanescent character of the surface modes. The second and less important mechanism is the chemical enhancement, for which different causes are discussed [5, 2, 6, 7]. Given the remarkable SERS enhancement, this technique can be used to sensitively determine highly dilute analytes [2]. In this regard, the reproducible fabrication of SERS substrates is an important field of plasmonic research and has yet to be developed. SERS substrates, which permit reliable determination of analytes, will drive SERS spectroscopy to a more application-oriented research area.

Reliable SERS substrates can be fabricated by e.g. electron beam lithography (EBL) [8]. In this case, the periodic alignment of silver or gold nanoparticles with a homogeneous size distribution results in reproducible SERS signals throughout the entire substrate area. However, the maximum sensitivity of these substrates is orders of magnitude smaller than what is needed for single molecule detection because of the relatively large gap spacings in between the plasmonically active nanoparticles. Smaller gap spacings can be realized using lithography techniques in combination with other nanostructuring techniques, e.g. atomic layer deposition or reactive ion etching [9, 10], furthermore in self-ordered arrays of spheres [11] or in nanosized (spherical) dimer structures [12, 13]. As long as they can be fabricated in a reproducible way, nanosized dimer structures (or dimer antennas) with gaps of a few nanometers provide an ideal SERS substrate due to the large and locally confined electromagnetic field enhancements [10].

At present, the EBL nanostructured substrates and functionalized metallic particles [11–13] are the main SERS substrates in use. However, while the gap spacings in the case of EBL use only remain relatively large, they are occupied with the necessary 'glue' in the case of functionalization [11–13]. To reliably fabricate dimer structures with the smallest gaps which can arbitrarily be filled, a direct writing method like the electron beam induced deposition (EBID) is advantageous. The EBID method provides for a highly accurate and precise fabrication of three-dimensional nanostructures ensuring structural details smaller than 20 nm [14].

For EBID a focused electron beam is used to crack a precursor gas which is inserted into the vacuum chamber of a scanning electron microscope (SEM). The deposition results from a local decomposition of the precursor molecules in the focal region of the electron beam onto the substrate surface (and accordingly onto the deposit surface) due to electron impact [14, 15]. All types of incident and scattered electrons contribute to the deposition, but preferentially the secondary electrons [16–18]. After decomposition, the non-volatile part of the precursor forms the deposit while the volatile remainder is pumped out of the vacuum chamber. The efficiency of the deposition is proportional to the density of molecules adsorbed at the surface and to the number of electrons in the deposition region [14, 15].

The used precursor gas dimethyl-gold(III)-acetylacetonate ($Me_2$acac) is of metal–organic nature and shows a gold-to-carbon ratio of 1:7 in its molecular formula. Thus, even in the pressure range below $10^{-6}$ hPa used for EBID, a low gold content of the deposits of approximately 15 at.% is expected and observed [19]. The gold forms nanocrystals with sizes of 2–7 nm in diameter which are dispersed in a carbonaceous matrix; this makes the EBID material a metamaterial in itself [20]. However, for SERS applications this carbonaceous matrix is disadvantageous since it hinders a free electron gas at the structure surface. To permit applications of EBID structures which require a pure metallic nature, purification techniques to remove the carbon from the deposits were developed [21, 20]. As an alternative to purifying EBID materials it is an option to add metallic coatings e.g. to dimer nanostructures. This approach is followed in this work. The EBID nanostructures are covered by thin silver layers (a few nanometers thick) by evaporation. The layer deposition moreover permits us to tune the resonant behavior of the EBID structures to be in resonance conditions with the analytes [22].

In this paper we present the fabrication of three-dimensional plasmonically active dimer antennas by electron beam induced deposition (EBID) and subsequent silver layer coating to be used in arrays as SERS substrates. EBID is well suited for the production of reliable and precise SERS substrates composed of periodic arrays of dimer antennas. Polarization dependent SERS measurements using the model dye methyl violet demonstrate the strong plasmonic activity of the silver-coated EBID antennas as well as the spatially homogeneous and reproducible SERS signal generation capabilities of these substrates.

## 2. Fabrication of the plasmonic dimer antennas

To achieve an optimum SERS enhancement and a minimum shadowing effect, dimer antennas that consist of two pillars are written by the EBID method onto silicon wafers. The pillars face one another and are inclined 45° with respect to

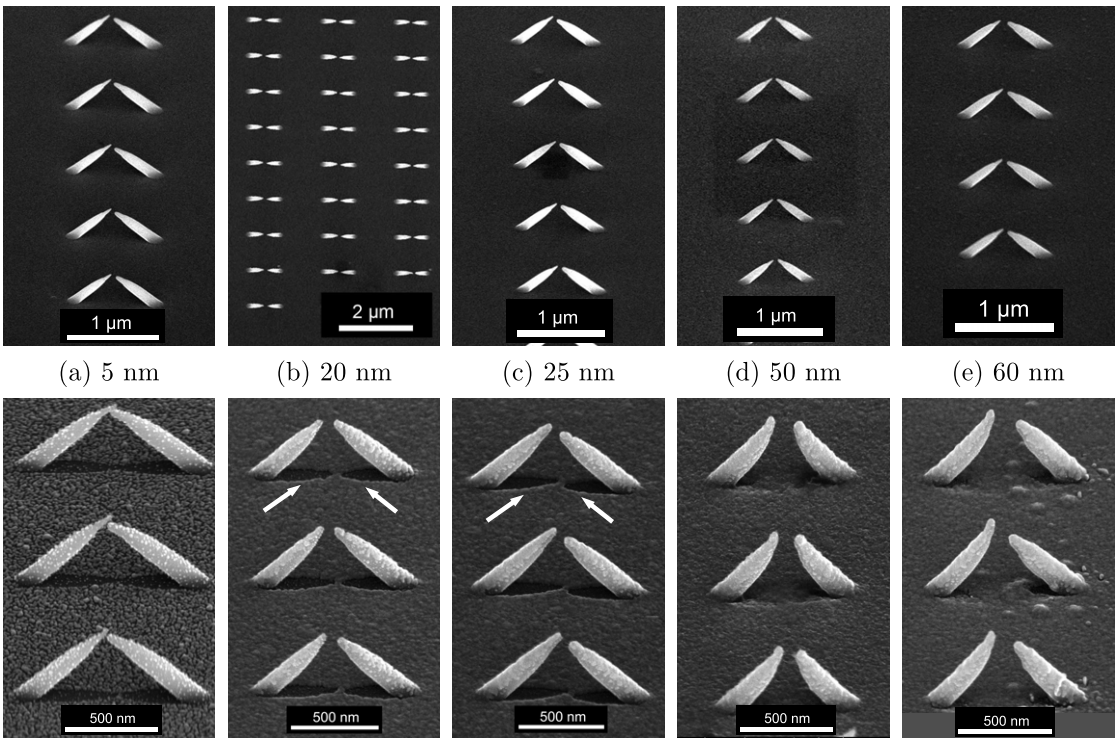


**Figure 2.** Scanning electron micrographs of pre-structured EBID substrates before (upper line) and after (lower line) the deposition of different silver thicknesses. The arrows indicate the geometric shadows of the directed silver vapor resulting in a reduced deposition. .

the substrate surface. At the closest point the EBID pillars assume tip radii of the order of 3–5 nm. The gap between these pillars can be reduced to ≈5 nm, which is as small as possible but wide enough so that no impingement of most pillars takes place. As precursor gases metal–organic precursor species like methyl-cyclopentadien-(trimethyl)-platin ($MePtCpMe_3$) or dimethyl-gold(III)-acetylacetonate ($Me_2acac$) were used for deposition. Typical EBID dimer structures (prior to silver layer coating) are shown in figure 1; these dimer antennas were fabricated using the standard precursor $MePtCpMe_3$.[5] The effective antenna length is ≈700 nm for light incidence from above, and each individual antenna shows a base radius of around 50 nm, i.e. larger than the tip radius, to ensure mechanical stability. The expected field enhancement in the hotspot of dimer antennas is maximum for excitation along the dimer axis, indicated by the double-headed arrow in the top view of figure 1. In this case, the most efficiently excitable long axis of the antenna [23] is combined with the likewise most efficiently excitable dimer axis [24] and a high curvature in the hotspot region.

The fabrication of the EBID dimer antennas was carried out using an FEI NovaNanolab dual beam instrument equipped with several gas injection systems (GIS), one equipped with $Me_2acac$ and one with $MePtCpMe_3$. Within a patterning routine the patterns can be defined varying several parameters such as pitch, beam dwell time, number of patterning loops etc [20]. Each pillar is individually written by EBID with the focused electron beam rendering a circular area of 30 nm radius for the pillar base and 5 nm radius for the pillar tip; the parameters of the electron beam are 15 keV and 0.14 nA with 729 $\mu$s dwell time. After depositing the first row of pillars onto the tilted silicon substrate followed by a 180° rotation, the second row is written such that the small gap arrangement is realized.

After EBID deposition of all pillars, plasmonic activation was carried out by coating the structures with a thin silver layer. For the substrates to be plasmonically activated, $Me_2acac$ as precursor gas was used and larger gap spacings were left. The spacings of the pillars in the gap region range from 20 to 60 nm, depending on the silver layer thickness. The thin silver layer was added using an Edwards thermal evaporator with a work pressure of $4 \times 10^{-4}$ hPa. Figures 2(a)–(e) show scanning electron micrographs of EBID antenna ensembles before and after the deposition of layers with different silver thicknesses. The experiments showed that a continuous silver layer on the EBID antennas is realized only for silver layer thicknesses of more than 25 nm. Thinner silver layers form islands on the carbon surface of the EBID dimers, as visible in figures 2(a) and (b).

Unfortunately, the evaporation process has certain unwanted consequences for the EBID antennas. With an increase of deposition time a shape change of the EBID antennas is observed, most likely caused by the radiative heat of the (up to ≈1000°C) evaporator boat hosting the silver. During the deposition the antenna tips start melting and creeping toward the pillar base. This can be recognized by the geometric shadows (indicated by arrows) underneath the

[5] This organometallic precursor has properties comparable to the later used $Me_2acac$ precursor, especially concerning the structural composition characterized by nanoparticles embedded in a carbonaceous matrix.

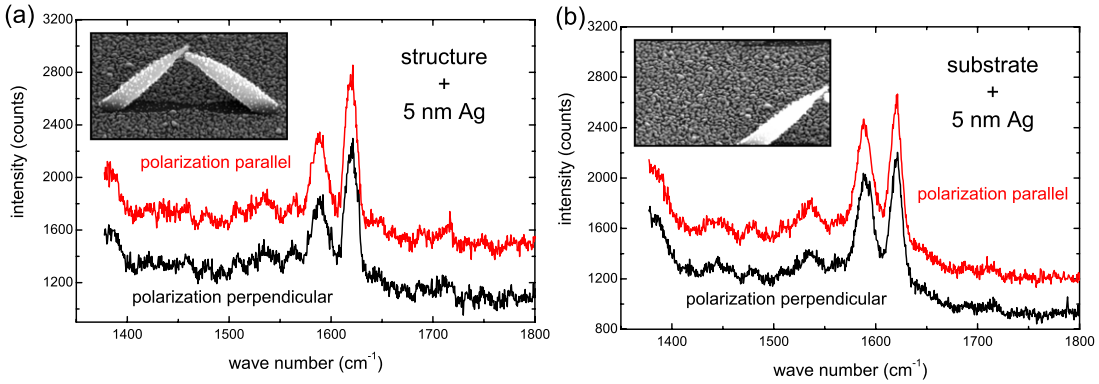


**Figure 3.** Typical Raman spectra of methyl violet (concentration tenfold increased) on a pre-structured silicon wafer with EBID antennas coated with 5 nm silver for a polarization along (red) and perpendicular to (black) the dimer axis. Since the silver forms separate islands instead of a continuous layer, the pre-structuring has no influence on the plasmonic enhancement of the surface; antenna region (a) and substrate region (b) show comparable Raman signals and thus enhancements.

EBID structures in figures 2(b) and (c), depicting the contours of the as-deposited EBID antennas. This melting increases the radius of curvature of the pillar tips as well as the gap spacings and therefore decreases the maximum possible field enhancement in the hotspot. Since the heat radiation affects mainly the upper structure surface of the thinner tips, these tips are bent upwards. To avoid this pillar shape change a substrate cooling or a modified evaporation chamber design could be introduced.

## 3. Raman measurements

The Raman measurements presented in this paper were performed using a Horiba Jobin Yvon LabRam HR 800 micro-Raman spectrometer under perpendicular incidence of laser light. For the SERS measurements the 514 nm emission line of an air cooled $Ar^+$ ion laser was used. Using 50× and 100× microscope objectives it is possible to focus the laser spot down to diameters of approximately 1.75 $\mu$m and 0.85 $\mu$m, respectively. Accordingly, the standard laser output power of around 20 mW creates an energy density of up to $\approx 2.5 \times 10^9$ W m$^{-2}$ locally on the sample surface which can cause heat damage of the EBID structures. To avoid any damage, neutral density filters of type D1 (10 times attenuation) and D2 (100 times attenuation) were used. For the polarization dependent SERS measurements, a $\lambda/2$ plate was used to align the linear polarized laser light into the desired positions[6]. With a movable $x$–$y$ sample stage, maps of the spatial distribution of the SERS intensities can be recorded for each polarization direction (parallel and orthogonal to the EBID dimer axes). The spatial resolution of the maps is limited by the size of the focused laser spot and due to potential focus drifts during the long term SERS measurements. To evaluate the SERS capabilities of the EBID dimer structures, the dye molecule methyl violet was used [25]. The SERS measurements were carried out using an aqueous solution of $10^{-5}$ mol l$^{-1}$ of the dye. To account for a monomolecular coverage of the dye, the SERS substrate was rinsed in the solution for 30 min prior to cleaning the substrate in deionized water.

To accurately determine the SERS enhancement factors of the EBID antennas, standard Raman measurements on an aqueous solution of methyl violet were performed for the setup described above, serving as a reference [26]. Without surface enhancement one single dye molecule contributes to the Raman signal rate

$$I_{\mathrm{RS}}^{\mathrm{single}} = 6.3 \times 10^{-7}\ \mathrm{s}^{-1} \qquad (1)$$

counts per second, corresponding to 18 days waiting time on average for a single event to occur.

## 4. SERS spectra

The following section presents the SERS spectra of methyl violet spread onto different EBID pre-structured and silver-coated SERS substrates. As a first example, the SERS spectra on a substrate with a non-continuous silver layer is shown in figure 3. The evaporated silver layer with a thickness of around 5 nm forms equally distributed silver islands with diameters in the range of 10 nm up to 25 nm (see also figure 2(a)). In this case the underlying EBID structures do not act as plasmonic antennas and therefore no special field enhancement is expected in the pre-structured region. Nevertheless, the silver islands give rise to a distinct surface enhancement everywhere on the substrate. The corresponding Raman measurements showed a relatively weak signal, so an increased concentration of methyl violet up to $10^{-4}$ mol l$^{-1}$ is required. Figure 3 shows typical spectra from individual Raman measurements with a recording time of 200 s using a 50× objective and a D2 neutral density filter. The (linear) polarization direction was chosen along the dimer axis (red spectra) and perpendicular to the dimer axis (black spectra). For comparison, not only the spectra in the antenna region (figure 3(a)), but also the spectra of the substrate region (figure 3(b)), are shown. As expected, figures 3(a) and (b) show no polarization dependence and no significant difference

[6] However, as the rotation of the linearly polarized laser light by a $\lambda/2$ plate also changed the shape and intensity of the laser spot, the incident polarization direction was kept fixed and the samples were rotated instead of the polarizer.

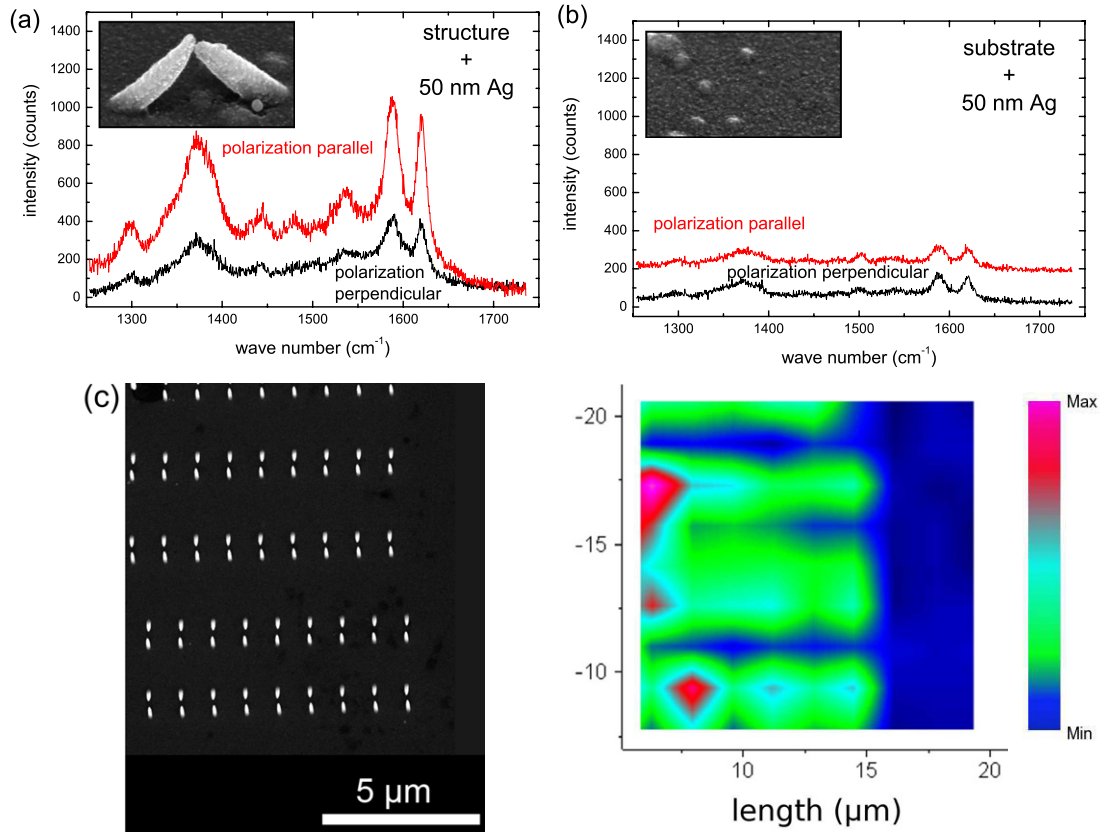


**Figure 4.** Typical Raman spectra of methyl violet taken from a mapping on EBID antennas coated with a 50 nm silver layer (a) in the dimer antenna region and (b) in the substrate region. In the substrate region the polarization dependent SERS intensity becomes maximum for polarization along the dimer axis (red). (c) Example of a mapping (on the sample shown in figure 2(d)) with a 50 nm silver layer; the scanning electron micrograph on the left shows the EBID antenna arrangement of the mapped region.

in signal intensity for the EBID antenna region compared to the substrate region. Individual silver islands on the substrates as well as on the EBID antennas provide for an equally distributed weak Raman signal enhancement throughout the entire sample, which is independent of the polarization.

This behavior changes once plasmonically active dimer antennas provide for localized Raman signal enhancements as shown in figure 4. The spectra in figure 4 represent typical spectra selected from a mapping of a sample which was coated with a 50 nm silver layer after the EBID antenna deposition using an aqueous solution of $10^{-5}$ mol $l^{-1}$ of methyl violet. The mapping was recorded using a 50× objective and a D1 filter in a region of 300 $\mu m^2$ with pixel spacings of 1.5 $\mu$m and a recording time of 30 s for each pixel.

Figure 4(a) shows two spectra of the antenna region after silver layer deposition; in figure 4(b) the corresponding spectra of the bare, silver-coated silicon substrate are shown. The polarization dependence is clearly visible in figure 4(a). Along the dimer axis the Raman bands of methyl violet are four times more intense compared to the perpendicular polarization. Furthermore, the silver-coated substrate shows no polarization dependence but a distinct Raman enhancement due to the nanoscale roughness of the silver layer[7].

[7] At this point it has to be mentioned that the spectra for the different directions of polarization cannot be correlated to a special position onto the substrate. The substrate was rotated to change the polarization direction.

A mapping of the sample in figure 2(d) again coated with a 50 nm thick silver layer is shown in figure 4(c) on the right; the corresponding scanning electron micrograph of the mapped region is shown on the left in figure 4(c). The mapping has pixel spacings of 1.5 $\mu$m with 60 s recording time for each individual Raman spectrum. Despite the relatively large dimer spacings, also visible in figure figure 2(d), the arrangement into lines is clearly visible. Furthermore, several single hotspots can be distinguished (red) and a strong decrease of signal intensity can be observed for the substrate region. An exact localization, however, is not possible due to the low spatial resolution of the mapping. Due to unavoidable mechanical vibrations of the complete setup, the very long acquisition time for a complete mapping causes a decreasing quality of focusing. This problem can be circumvented by carefully placed linescans, which allow us to double the recording time to 120 s for each spectrum. Again, the pixel distance was 1.5 $\mu$m for the separate spectra using the 50× objective and the stronger D2 filter to avoid any heat degradation of the plasmonic antennas.

Figure 5 shows typical spectra from such linescans for plasmonic dimer antennas coated with a 40 nm silver layer. The two recorded spectra in figure 5(a) originate from one and the same line of antennas excited using parallel and perpendicular polarization of the laser light. Thus, it is possible to address spectra of both polarization directions to

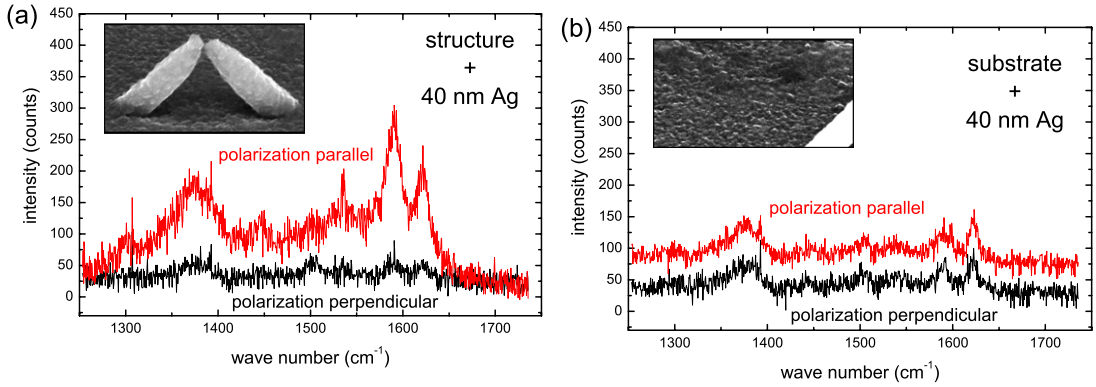


**Figure 5.** Typical Raman spectra of methyl violet taken from a linescan of an EBID pre-structured sample with a 40 nm silver coating (a) in the dimer antenna region and (b) in the substrate region for polarization along (red) and perpendicular (black) to the dimer axis.

identical dimer antennas. The spectra in figure 5(a) again show a four times higher Raman signal for the polarization along the dimer axis compared to excitation perpendicular to the dimer axis.

## 5. Estimation of Raman enhancements

Currently, no standard method for the determination of Raman enhancement factors [4] is established. Following the suggestions of Cai [26, 4], the enhancement factors $f$ of the spectra shown in this work were estimated following

$$f = \frac{1}{I_{\mathrm{RS}}^{\mathrm{single}}} \frac{I_{\mathrm{SERS}}}{N_{\mathrm{CV}} \cdot t}, \qquad (2)$$

with $I_{\mathrm{RS}}^{\mathrm{single}}$ (cf 1) constituting the experimentally determined non-SERS Raman intensity for a single dye molecule per second, with the measured SERS intensity $I_{\mathrm{SERS}}$ corrected by the intensity reduction by the filters (not shown) and normalized to the number of excited molecules $N_{\mathrm{CV}}$ within the laser spot and the recording time $t$ for the spectra. For this estimation the intensities, the recording times and as well the dimensions of the laser spot are experimentally accessible; in contrast the determination of the number of excited molecules $N_{\mathrm{CV}}$ is problematic. A reliable estimation is possible only in the case of single molecule spectra, requiring distinctly higher enhancement factors.

For conventional SERS measurements as carried out in this paper usually a monolayer of dye molecules is assumed to be adsorbed onto the substrate [8]. With an occupied area of 3.51 nm$^2$ per molecule [27], around 680 000 molecules are adsorbed in the laser spot area of around 2.4 $\mu$m$^2$ for the used 50× objective[8].

Table 1 shows the estimated enhancement factors for spectra from mappings and linescans as shown in figures 4 and 5 using the assumptions concerning $N_{\mathrm{CV}}$. Therein, the enhancement factors for the silver-coated substrate (without EBID pre-structuring) are already as high as for periodically arranged gold nanostructures [8]. On the other hand, the pre-structured antenna region shows enhancement factors of the order of $1 \times 10^3$. Since the plasmonic dimer antennas only cover about 5% of the pre-structured substrate surface (cf figures 2(b) and 4(c)), the enhancement factor of the plasmonic dimer antennas themselves should be distinctly higher. For the assumption of a uniform molecule coverage a simple formula is deduced:

$$f_{\mathrm{ant+sub}} = \frac{A_{\mathrm{sub}}}{A_{\mathrm{ant+sub}}} \times f_{\mathrm{sub}} + \frac{A_{\mathrm{ant}}}{A_{\mathrm{ant+sub}}} \times f_{\mathrm{ant}}$$

using the ratios of the areas $A_{\mathrm{sub}}$ and $A_{\mathrm{ant}}$ of the bare substrate and the dimer antennas to the area $A_{\mathrm{ant+sub}}$ of the pre-structured region. With $f_{\mathrm{ant+sub}} \approx 4 \times f_{\mathrm{sub}}$ an enhancement factor of

$$f_{\mathrm{ant}} \approx 1.2 \times 10^4$$

results for the plasmonic dimer antennas excited along the dimer axis. This value is comparable to the enhancement of planar, plasmonically coupled gold antennas [28] in which the lattice constant and dimensions of the single antennas were chosen such that the plasmon resonant behavior matched the absorption maximum and Stokes shift for the characteristic band of methyl violet at 1620 cm$^{-1}$. However, for the proposed silver dimer antennas the obtained SERS enhancement is not optimal. One reason may be loss effects due to the underlying EBID material, since the excitation wavelength $\lambda = 514$ nm matches the (mostly absorptive) plasmon resonance of the tiny gold nanocrystals embedded into the EBID material. Thus, future tasks include the tuning of the resonance positions of the presented dimer antennas via different thicknesses of the plasmonic silver layer to match

**Table 1.** Estimation for the enhancement factors of the representative spectra from mapping and linescan shown in figure 4 and 5.

| Figure 4: mapping, 50 nm Ag | | Figure 5: linescan, 40 nm Ag | |
|---|---|---|---|
| Substrate | Antennas + substrate | Substrate | Antennas + substrate |
| 160 | 1000 | 230 | 600 |

[8] We did not differentiate between the antenna region and substrate region, because the plasmonically activated areas are comparable in the antenna region and in the substrate area, due to the shadowing effects arising during the silver evaporation (cf figure 2).

both an optimal laser excitation wavelength and the resonance positions of the analytes. This way an improved enhancement factor by orders of magnitude is expected.

## 6. Conclusions

In this paper the surface enhanced Raman scattering (SERS) on plasmonic dimer antennas is presented. These antennas are fabricated by electron beam deposition (EBID) and thus represent the first spectroscopic application of the EBID technique. In contrast to other fabrication methods, EBID allows for the highly reproducible direct writing of three-dimensional nanostructures. These capabilities were used to fabricate free-standing dimer antennas which face one another with their tips and form a small gap, the so-called hotspot region, that can be filled arbitrarily with analytes of interest. The long axes of the individual antennas are oriented along the dimer axis (but inclined by 45° with respect to the substrate surface), and thus a high excitation efficiency along these axes is expected.

After writing the EBID dimer antennas a plasmonic activation becomes necessary due to a substantially high carbon content within the deposits. Therefore, a deposition of thin silver layers onto the EBID structures and the entire substrate surface was carried out. After this activation procedure, the structured substrates constitute the so-called SERS substrate for subsequent spectroscopy of analytes of interest. The substrates were assessed for the SERS application using methyl violet as a model analyte and estimations of the achieved Raman signal enhancement factors are given. Polarization dependent Raman measurements prove the expected strong signal enhancement for the coupling of the elongate antennas constituting the dimer. For an incident polarization of the laser light along the dimer axis, corresponding to the case of optimal dimer coupling, enhancement factors of the order of $10^4$ were achieved.

While this study is only a proof of concept for the applicability of EBID in plasmonics, future attempts can significantly improve the antenna's signal enhancement capabilities by systematic use of the silver coating for tuning of the plasmon resonant behavior.

## Acknowledgments

The authors thank Dr H Blumtritt and Mr N Schammelt for technical assistance with the dual-beam instrument, Nadine Geyer and Jörg Wittemann for silver coating the EBID structures and Hilmar Straube for the fruitful discussions. This work was supported by the European Commission within the project 'FIBLYS' (FP7-NMP-214042) and within the joint Max Planck Society–Fraunhofer Society project 'Nanostress'.

## References

[1] Schuller J A, Barnard E S, Cai W, Jun Y C, White J S and Brongersma M L 2010 *Nature Mater.* **9** 193–204
[2] Kneipp K, Kneipp H, Itzkan I, Dasari R and Feld M 2002 *J. Phys.: Condens. Matter* **14** R597–624
[3] Kneipp K, Kneipp H and Moskovits M 2006 *Surface-Enhanced Raman Scattering* (Berlin: Springer)
[4] Le Ru E C, Blackie E, Meyer M and Etchegoin P G 2007 *J. Phys. Chem.* C **111** 13794–803
[5] Moskovits M 1985 *Rev. Mod. Phys.* **57** 783–826
[6] Persson B N J, Zhao K and Zhang Z 2006 *Phys. Rev. Lett.* **96** 207401
[7] Le Ru E C, Etchegoin P G and Meyer M 2006 *J. Chem. Phys.* **125** 204701
[8] Cialla D, Huebner U, Schneidewind H, Moeller R and Popp J 2008 *ChemPhysChem* **9** 758–62
[9] Im H, Bantz K C, Lindquist N C, Haynes C L and Oh S H 2010 *Nano Lett.* **10** 2231–6
[10] Hatab N A, Hsueh C H, Gaddis A L, Retterer S T, Li J H, Eres G, Zhang Z and Gu B 2010 *Nano Lett.* **10** 4952–5
[11] Wang Z and Rothberg L 2005 *J. Phys. Chem.* B **109** 3387–91
[12] Talley C, Jackson J, Oubre C, Grady N, Hollars C, Lane S, Huser T, Nordlander P and Halas N 2005 *Nano Lett.* **5** 1569–74
[13] Lim D K, Jeon K S, Kim H M, Nam J M and Suh Y D 2010 *Nature Mater.* **9** 60–7
[14] Utke I, Hoffmann P and Melngailis J 2008 *J. Vac. Sci. Technol.* B **26** 1197–276
[15] Randolph S, Fowlkes J and Rack P 2006 *Crit. Rev. Solid State Mater. Sci.* **31** 55–89
[16] Hoyle P, Cleaver J and Ahmed H 1996 *J. Vac. Sci. Technol.* B **14** 662–73
[17] Fischer M, Wanzenboeck H, Gottsbachner J, Muller S, Brezna W, Schramboeck M and Bertagnolli E 2006 *Microelectron. Eng.* **83** 784–7
[18] Fowlkes J, Randolph S and Rack P 2005 *J. Vac. Sci. Technol.* B **23** 2825–32
[19] Botman A, Mulders J J L, Weemaes R and Mentik S 2006 *Nanotechnology* **17** 3779–85
[20] Höflich K, Yang R B, Berger A, Leuchs G and Christiansen S 2011 *Adv. Mater.* **23** 2657–61
[21] Botman A, Mulders J J L and Hagen C W 2009 *Nanotechnology* **20** 17
[22] Halas N 2005 *MRS Bull.* **30** 362–7
[23] Barnard E S, White J S, Chandran A and Brongersma M L 2008 *Opt. Express* **16** 16529–37
[24] Ringler M, Schwemer A, Wunderlich M, Nichtl A, Kuerzinger K, Klar T A and Feldmann J 2008 *Phys. Rev. Lett.* **100** 203002
[25] Watanabe T and Pettinger B 1982 *Chem. Phys. Lett.* **89** 501–7
[26] Cai W, Ren B, Li X, She C, Liu F, Cai X and Tian Z 1998 *Surf. Sci.* **406** 9–22
[27] Iqbal M J and Ashiq M N 2010 *J. Chem. Soc. Pak.* **32** 419–28
[28] Petschulat J *et al* 2010 *Opt. Express* **18** 4184–97